8-1-2002

The 1.20 Å Resolution Crystal Structure of the Aminopeptidase from *Aeromonas proteolytica* Complexed with Tris: A Tale of Buffer Inhibition

William Desmarais
Brandeis University

David L. Bienvenue
Utah State University

Krzysztof P. Bzymek
Utah State University

Richard C. Holz
Marquette University, richard.holz@marquette.edu

Gregory A. Petsko
Brandeis University

See next page for additional authors

Accepted version. *Structure*, Vol. 10, No. 8 (August 2002): 1063-1072. DOI.
Richard Holz was affiliated with the Utah State University at the time of publication.

Structure, Vol. 10, No. 8 (August 2002): 1063-1072. DOI.

The 1.20 Å Resolution Crystal Structure of the Aminopeptidase from *Aeromonas proteolytica* Complexed with Tris: A Tale of Buffer Inhibition

William T Desmarais
Program in Biophysics and Structural Biology, Waltham, MA 02454 USA

David L Bienvenue
Utah State University, Logan, UT 84322 USA

Krzysztof P Bzymek
Utah State University, Logan, UT 84322 USA

Richard C Holz
Utah State University, Logan, UT 84322 USA

Gregory A Petsko
Departments of Chemistry and Biochemistry, Waltham, MA 02454 USA
Rosenstiel Basic Medical Sciences Research Center, Brandeis University, Waltham, MA 02454 USA

Dagmar Ringe
Departments of Chemistry and Biochemistry, Waltham, MA 02454 USA
Rosenstiel Basic Medical Sciences Research Center, Brandeis University, Waltham, MA 02454 USA

Abstract

The aminopeptidase from *Aeromonas* proteolytica (AAP) is a bridged bimetallic enzyme that removes the N-terminal amino acid from a peptide chain. To fully understand the metal roles in the reaction pathway of AAP we have solved the 1.20 Å resolution crystal structure of native AAP (PDB ID = 1LOK). The high-quality electron density maps showed a single Tris molecule chelated to the active site Zn^{2+}, alternate side chain conformations for some side chains, a sodium ion that mediates a crystal contact, a surface thiocyanate ion, and several potential hydrogen atoms. In addition, the high precision of the atomic positions has led to insight into the protonation states of some of the active site amino acid side chains.

Keywords

Metalloenzyme, aminopeptidase, zinc, tris, high resolution, buffer inhibition

Introduction

Bimetallohydrolases are a class of enzymes that utilize two metal ions connected by a bridging ligand to catalyze hydrolytic reactions. Their ability to catalyze such diverse reactions as the degradation of DNA, RNA, phospholipids, and polypeptides 1, 2, 3, 4 make them key players in carcinogenesis, tissue repair, protein maturation, cell cycle control, hormone-level regulation, and protein degradation. These enzymes are also involved in the degradation of agricultural neurotoxins, urea, antibiotics, and several phosphorous(V) materials used in chemical weaponry 5, 6, 7.

Binuclear metallo-aminopeptidases are enzymes that catalyze the hydrolysis of N-terminal amino acid residues from proteins and polypeptides. They can be grouped into two major types. One type is highly specific and removes a particular N-terminal amino acid from a peptide or protein, a process required for protein maturation. The bimetallic enzyme, proline aminopeptidase (AMPP), is a member of this type. In rat, membrane-bound AMPP has been implicated as a kininase, degrading the vasodilator bradykinin in the rat pulmonary vascular bed, in the rat heart, and in the human skin [8]. The second type of aminopeptidase is relatively nonspecific and removes most any amino acid from the N terminus of a peptide 9, 10. These enzymes are commonly involved in the general degradation of peptides and proteins. In mammals, abnormal aminopeptidase activity has been linked to health conditions such as aging, cataracts, inflammation, cystic fibrosis, cancer, and leukemia 9, 10. These conditions may be a result of improper protein maturation, but are most likely due to aberrant general protein degradation. One enzyme in this class, leucine aminopeptidase, is targeted by the naturally occurring peptide analog, bestatin, resulting in a decrease of HIV infection in males [11].

As a model for bimetallohydrolases in general and for enzymes that cleave N-terminal amino acids from peptides in particular, we have been studying the aminopeptidase from *Aeromonas proteolytica* (AAP). AAP is a small, relatively nonspecific, secreted, dizinc monomeric enzyme (32,000 Da) that is thermostable for several hours at 70°C [12]. The crystal structure of AAP at 1.8 Å resolution revealed a single α/β globular domain with a centrally located mixed β sheet sandwiched between two α helices [13]. The active site of AAP is composed of a (μ-aqua)(μ-carboxylato)dizinc(II) catalytic core (Figure 1). It is important to note that although the bridging water species has been described previously as a water molecule (H_2O), the actual protonation state is unknown. It is at least equally likely that the bridging water is actually a bridging hydroxy anion (OH^-). Both Zn(II) ions have a distorted tetrahedral coordination geometry with a Zn-Zn distance of 3.5 Å. Each metal ion is coordinated to a side chain carboxylate and a histidine residue, and both metals are required for full catalytic activity. As in all bimetallic enzymes, the exact role of each metal ion in AAP is unknown. When only one metal ion is present,

AAP retains 80% of its catalytic activity 14, 15, and it has been proposed that the second metal ion is primarily utilized to stabilize the bridging water species and an intermediate in the chemical reaction pathway [16].

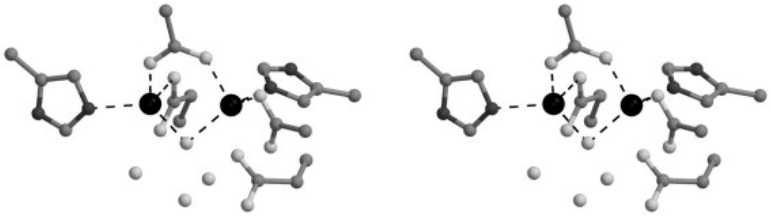

Figure 1. Active Site of AAP Solved to 1.8 Å Resolution

The protein is oriented so that the view is from the solvent looking into the active site and will be the same for all figures.

A mechanism for the enzymatic reaction of AAP has been proposed that relies on structural and spectroscopic information from the resting enzyme as well as the inhibited forms [17](Figure 2). Initially, the substrate binds to AAP by coordination of the carbonyl oxygen to Zn_1^{2+} and, in a second step, the N-terminal amine to Zn_2^{2+}. The metal-activated water molecule then attacks the scissile bond at the carbonyl carbon resulting in the formation of the gem diolate that is now stabilized by interactions with both zinc ions. The active site residue, Glu_{151}, may accept a proton from the bridging water molecule and then transfer it to the penultimate amino nitrogen of the new N terminus. Finally, the enzyme returns to its native state upon the release of products and the addition of a new bridging water molecule. The roles of Zn_2, in this mechanism, may be to stabilize the bridging water molecule, to assist in stabilizing the reaction intermediates, and to recognize and orient the substrate.

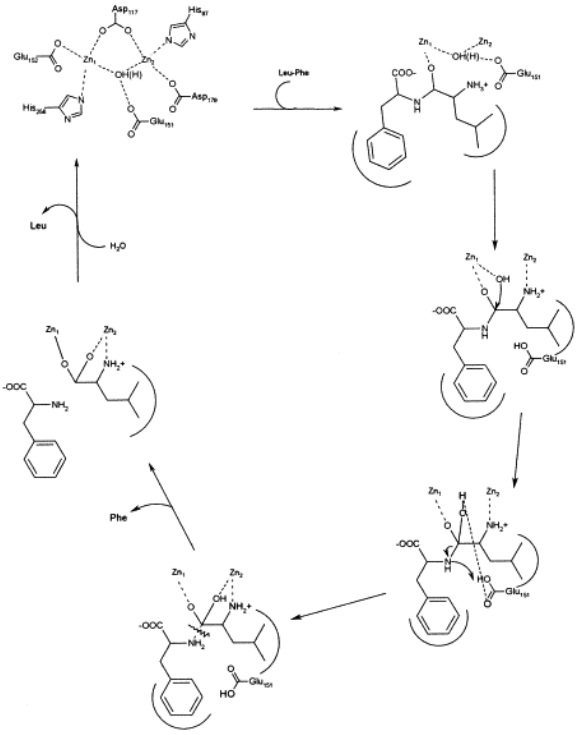

Figure 2. The Chemical Reaction Mechanism of AAP Based on Inhibited Structures of AAP and Spectral Analysis

For clarity, the metal-coordinating amino acid side chains are only included in the first step of the reaction mechanism.

Completely understanding the exact roles of the two metal ions in the reaction pathway of AAP with respect to substrate recognition and specificity, substrate binding, formation and degradation of intermediates, and product release requires precise knowledge of the position of every atom in the active site, including the positions of the hydrogens. For native unliganded AAP at 1.8 Å resolution, the positions and orientations of the active site amino acids and metal ions are known to a precision of about 0.17 Å [13]. The spectroscopic and kinetic data, and the inhibitor-bound crystal structures of AAP have allowed us to infer the roles of the active site amino acids and metals at each step in the reaction pathway, but without any direct experimental evidence as to the hydrogen positions, we are forced to assume the protonation states of the metal ligands, the bridging water molecule, and Glu_{151}.

Two very important hydrogens are those attached to the bridging oxygen. The bridging oxygen has previously been described as a water molecule (H_2O) 13, 16; however, to perform the peptide hydrolysis step in the reaction pathway, it must be converted to at least a hydroxonium ion OH^-. Coordination of a water molecule to a metal ion significantly decreases its pKa. A single zinc ion can lower the pKa of a water molecule in bulk solvent from 15.7 to 9.0 [18], while two zinc ions can lower it even further. At the pH range over which AAP has optimal activity (pH 7.5–9.0), the bridging oxygen may contain two protons (H_2O) or a single proton (OH^-).

Because of their low X-ray scattering, the positions of the hydrogen atoms are not observed directly in protein crystal structures carried out at typical resolution (3–1.5 Å). To directly observe hydrogens in an electron density map, a resolution of about 0.7 Å is required; however, some hydrogens can be observed at 1.20 Å resolution. Ultrahigh-resolution (1.0 Å or higher) X-ray diffraction also gives a more precise view of hydrogen bonds, cofactor geometry, and thermal disorder. As the first step toward determining the protonation states of the metal ligands, the bridging water molecule, and Glu_{151} in AAP, we have determined the 1.20 Å resolution structure of native AAP in the Tris containing buffer previously used to crystallize the enzyme (PDB ID = 1LOK). This high-resolution structure has led to a very precise analysis of AAP's active site and the discovery of a single Tris molecule chelated to the two metal ions. Because of the quality of the electron density maps at this resolution, the anisotropic treatment of thermal motion during refinement, and the cryogenic temperature used for data collection, we have also been able to model alternate side chain conformations.

Results and Discussion

Model of AAP at 1.20 Å Resolution

To date, crystallographic studies of bimetalloenzymes have focused primarily on native enzymes and analogs of the transition states at moderate resolutions (~2.0 Å). None of the crystallographic, biochemical, or spectroscopic evidence have been able to clearly identify the protonation states of the bridging water species nor the active site amino acids. In the case of AAP, no evidence has been provided to support the proposed role of Glu_{151} as the proton shuttle that receives a proton from the bridging water and then delivers it to the penultimate nitrogen. Recently, ultrahigh-resolution X-ray crystallography (~1.00 Å resolution) has been utilized to determine precise atomic positions and locate catalytically important hydrogens in a few enzymes [19]. We have applied this technology to AAP.

By utilizing shorter wavelength X-rays (1.00 Å), we have collected a 99% complete data set of native AAP to 1.20 Å resolution. There were no major conformational changes between the two high-resolution structures, with an rms deviation of 0.26 Å for the 291 structurally equivalent C_α atoms. There is a marked increase in the quality and detail of the electron density map relative to the same structure at 1.8 Å resolution (PDB ID = 1AMP). Over 98% of the protein residues are visible in an electron density map with coefficients $2F_{obs}$-F_{calc} at the level of 1.6 σ. The residues that are not visible are in flexible surface loop regions of the protein. In the well-ordered regions of the structure, the atom positions are represented by resolved electron density peaks of 5.0–8.5 σ. The high definition of the electron density in the bound solvent regions allowed for the detection of bound small

molecules that were not previously assigned at 1.8 Å resolution. In addition, the quality of the electron density is sufficiently high that the chemical identity of individual atoms can be determined by their integrated electron density.

Similar to the previously reported structure of AAP at room temperature, the 1.20 Å resolution structure of AAP at −173°C folds into a single α/β globular domain with a centrally located, mixed β sheet sandwiched between two α helices. The fine detail of the electron density map and the precise measurements in the atomic positions have allowed us to identify features of the structure that were not apparent at 1.8 Å resolution. On the surface of the protein we have identified a metal ion that coordinates via a water network to a second protein molecule, and a thiocyanate ion that is a component of the crystallization buffer. The cryogenic temperature at which the data were collected and the anisotropic treatment of thermal motion have enabled us to observe electron density corresponding to atoms that occupy multiple positions. Additionally, electron density corresponding to calculated hydrogen positions has been observed on some amide nitrogens and some amino acid side chains. At 1.8 Å resolution in a HEPES buffer, a network of four water molecules, one of which was the bridging water molecule, was described in the active site of AAP [13]. The fine detail of our 1.20 Å resolution electron density map also shows four spheres of electron density, in a similar location as those found in the 1.8 Å resolution structure, that are connected and correspond to a molecule of Tris (see below). The final model of our structure consists of 291 amino acids, 348 water molecules, two zinc ions, one sodium ion, one thiocyanate ion, and a molecule of Tris.

The final model was checked for accuracy by determining the conformationally favored geometry around each amino acid. The Ramachandran plot shows that 88.4% of the non-glycine residues are located in most favored regions of the conformational space. The remaining residues lie in the additional allowed regions with the exception of Met_{180}, which is located in a generously allowed region. The average ω angle for peptide bonds is 179.5° (standard deviationSD= 5.8) compares well to the value expected for ω angles of peptide bonds (ω = 178°, SD = 5.5).

Alternate Conformations of Side Chains

At 1.8 Å resolution, the thermal motion of atoms could only be modeled using an isotropic treatment of the thermal parameters, making it impossible to model side chain disorder. At 1.20 Å resolution, anisotropic treatment of the temperature factors is possible for every atom in the structure. Discrete alternate conformations can be observed for 15 side chains, 5% of the total amino acids in AAP. Of the 15 amino acids, 14 are either polar or charged, with 1/3 being serine side chains. The majority of these amino acids are located in loop regions of the protein, and none of them are directly implicated in enzyme catalysis. For example, the entire side chain of Arg_{156} occupies two conformations with approximately 50% occupancy for each (Figure 3). In one conformation, a terminal nitrogen interacts through a water network with the carbonyl oxygen of Ser_{71}, a side chain oxygen of Asp_{160}, and the phenolic oxygen of Tyr_{73}. In the alternate conformation, the same nitrogen interacts with a single water molecule. Arg_{156} is located on the surface of the enzyme and makes no contacts with other protein molecules in the unit cell.

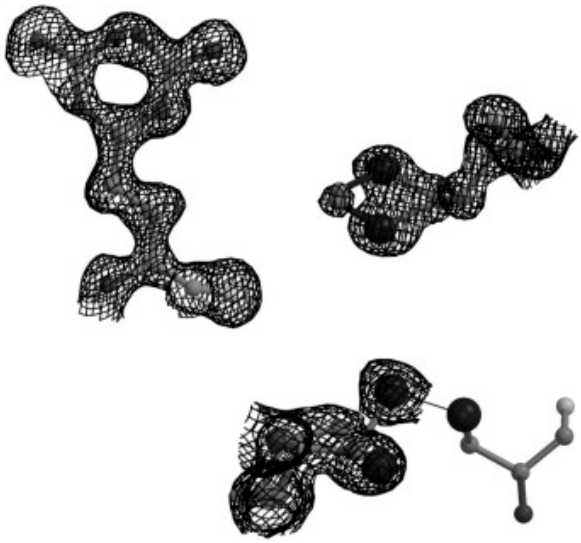

Figure 3. Alternate Side Chain Conformations of Arg_{156}, Met_{209}, and Cys_{223}

For clarity, the electron density for Cys_{227} was not included.

The disorder in Met_{209} is quite different from that of Arg_{156}. All of the atoms in Met_{209} occupy a single conformation with the exception of the side chain sulfur atom (Figure 3). The sulfur atom of Met_{209} appears to flip between two conformations via a 66° rotation about the C_α-C_β bond. Met_{209} is located in a hydrophobic cavity but does not have any interactions with other atoms in either conformation. Another amino acid, Cys_{223}, has a second conformation that is the result of a break in AAP's only disulfide bond, which is located at the back edge of the active site. In the alternate conformation, the sulfur atom of Cys_{223} interacts with a molecule of water, the carbonyl oxygen of Tyr_{225}, and the sulfur atom in Cys_{227}(Figure 3). The break in the disulfide bond is most likely the result of oxidation of the sulfur atom by a species generated by the highly intense synchotron X-rays used during the data collection. The role of the disulfide bond is unknown; however, it may be essential to bind substrate or to maintain the structural integrity of the active site [13].

Surface Structure

The detail of the electron density maps has allowed for the assignment of bound water and nonwater species; the latter includes a sodium ion Na^+, a thiocyanate ion (SCN^-), and a molecule of Tris. The solvent content of the crystal is 50% (v/v), which corresponds to approximately 455 fully occupied “theoretical” waters per asymmetric unit. In the final model, a total of 348 water molecules were included, with 338 water molecules refined at full occupancy and 10 refined at partial occupancy; approximately 76% of the total expected number of waters were located. The majority of the solvent content is well ordered with an average B value of 32.4 $Å^2$ for water molecules and 21.8 $Å^2$ for nonwater solvent molecules.

Water molecules that made at least one hydrogen bonding interaction with a protein atom were grouped into the first hydration shell, and those that had no hydrogen bonding interactions with the protein but did have hydrogen bonding interactions with other water molecules were grouped into the second hydration shell and higher. Using cut offs for hydrogen bonding donor-acceptor distances between 2.3 and 3.6 Å, 216 water molecules were located in the first hydration shell, while 132 were distributed in higher shells. The majority of the water molecules within hydrogen bonding distance to the protein made one contact to protein atoms, while only four water molecules made four potential contacts. The average B values of these water molecules decrease from 32 $Å^2$ for those making one contact with the protein to 21 $Å^2$ for those making four potential protein contacts. Water molecules in higher shells show a similar trend of decreasing B values as the number of hydrogen bonds to other waters increases. Twice as many water molecules made hydrogen bonding interactions

with main chain and side chain CO groups than with NH groups. Additionally, the average hydrogen bonding distance to the main chain and side chain nitrogen atoms (3.05 Å) was longer than that to the main chain and side chain oxygen atoms (2.95 Å). These results are consistent with previous findings that CO groups have a higher capacity to form hydrogen bonds than NH groups [20].

In the first hydration shell, five distinct electron density peaks and a tyrosyl oxygen peak from Tyr_{218} surrounded one well-defined electron density peak with distorted octahedral geometry (Figure 4). The structure reported to 1.8 Å resolution did not report a similar finding [13], however, an inspection of the atomic coordinates deposited in the Protein Data Bank revealed a network of six water molecules connected by a centrally located seventh water molecule with distorted octahedral geometry in the same location as the electron density observed in the 1.20 Å resolution structure. Considering that water molecules typically do not interact with more than four other atoms, the assignment of the central atom was most likely incorrect. AAP was crystallized in a solution that contained a high concentration of potassium and sodium ions, both of which can coordinate ligands octahedrally. The expected oxygen distances for Na-O and K-O are approximately 2.4 and 2.7 Å respectively for small molecule structures (B. Foxman, personal communication). At 1.8 Å resolution, the distances from the central atom to its six ligands range from 2.5 to 2.9 Å, which is closer to the expected K-O bonding distance. Nevertheless, the identity of the central atom remains unclear because the precision of the bond distances (0.17 Å) is not good enough to distinguish between K-O and Na-O bonds. At 1.20 Å resolution, however, the refined internuclear distances from atoms placed into each density peak in the 1.20 Å resolution structure ranged from 2.31 to 2.55 Å and are consistent with the expected value for a Na-O bond. The precision in these distances is good enough to identify the central atom as a Na^+. The monovalent cation lies at the interface of two protein molecules that are connected through the Na^+ by a network of water molecules. This electron density that we have interpreted as a Na^+ ion seems to be conserved in several AAP structures and may be essential in crystal packing (our unpublished data).

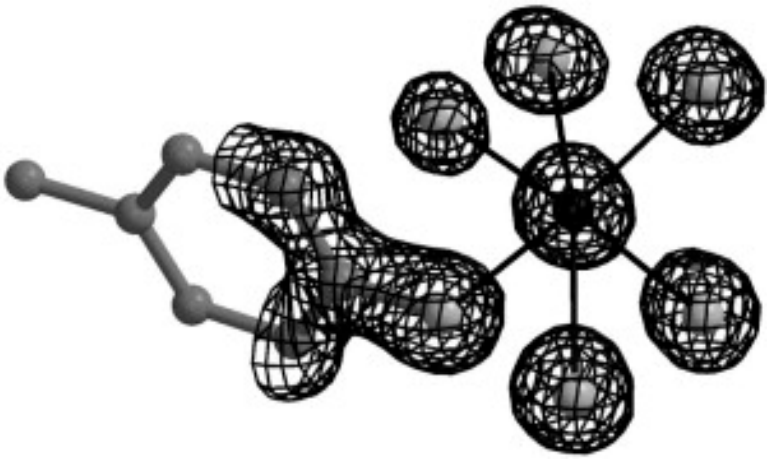

Figure 4. Octahedral Cordination Geometry of a Surface Na^+ Ion

The ligands to the Na^+ ion are five water molecules and the phenolic oxygen from Tyr_{218}.

A feature of the electron density that can only be interpreted as a SCN^- is located in a small binding pocket on the surface of the protein. The molecule makes two direct contacts and, through a water network, makes two indirect contacts with the protein (Figure 5). The negative charge is stabilized by interactions with the side chain of Asn_{171} and a water molecule. The direction of binding of the SCN^- is distinguishable because the electron density for sulfur is larger than that for the other atoms. SCN^- may be present at 1.8 Å resolution; however, the quality of the data allowed for only one of the atoms to be found, and it was interpreted as a water molecule [13].

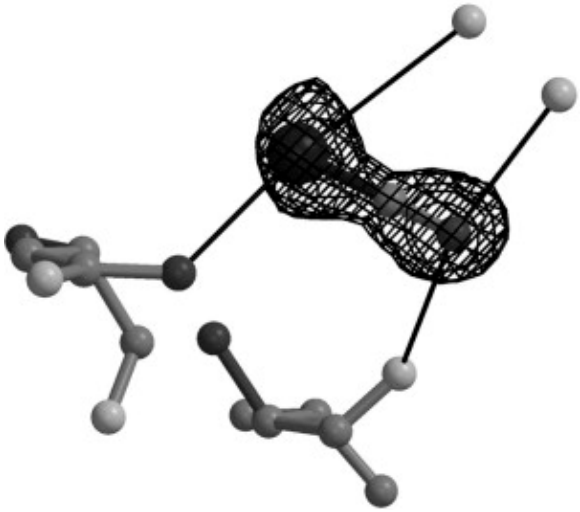

Figure 5. Electron Density of a SCN^- Ion Located on the Surface of the Enzyme

The Active Site

The active site showed two very well-formed spheres of electron density that remained visible up to the 40 σ level in a difference Fourier electron density map with coefficients $2F_{obs}$-F_{calc}. These corresponded to the two zinc ions that are located 3.45 Å apart. As shown in the 1.8 Å resolution structure, both metal ions have tetrahedral coordination geometry with each metal ion coordinating a bridging carboxylate, a bridging oxygen, a carboxylate side chain, and an imidazole side chain. The positions of the two metal ions were not restrained during refinement allowing precise Zn-ligand distances to be obtained without bias. The ligands to the zinc ions can be classified into two types: those that coordinate in the first coordination sphere of the metal ion and those that coordinate in the second and higher coordination spheres. In the case of AAP, a ligand to Zn^{2+} is considered in the first coordination sphere if the Zn-X distance is less approximately 2.1 Å. The second coordination sphere of Zn^{2+} is difficult to assign but typically starts with ligand distances of approximately 2.3 Å. For AAP, the two oxygen atoms from Asp_{117}, one oxygen each from Glu_{152} and Asp_{179}, and both ϵ nitrogens from His_{97} and His_{256} are in the first coordination sphere, while the second oxygens of Glu_{152} and Asp_{179}, known as the dangling oxygens, are in the second coordination sphere (Table 1). In the first coordination sphere, the average Zn-N distance is 2.08 Å, and the average Zn-O distance is 2.05 Å, while in the second sphere, the oxygens have a longer average Zn-O distance of 2.37 Å.

Table 1. Statistics of X-Ray Diffraction Data and Structure Refinement

Data Set	Edge	Peak	Remote
Wavelength (Å)	1.28210	1.28140	1.0500
Resolution (Å)	15.0–1.6	15.0–1.6	15.0–1.6
Redundancy	4.38	4.36	2.16
Unique reflections	62080	62044	62025
Completeness overall (%)	99.9	99.9	98.8
Outermost shell (%) (1.63–1.60)	99.2	99.2	93.3
I/σ	22.69	23.48	16.15
R_{sym}[a] (%)	7.6	6.8	6.1

a

$$R_{sym} = \Sigma_{hkl}\Sigma_i|I_{hkl,i} - \langle I\rangle_{hkl}|/\Sigma|\langle I\rangle_{hkl}|$$

The distribution of the double bond of the zinc-liganded carboxylates can have three possible configurations, it can be distributed equally among the two oxygen atoms, localized to the first sphere zinc-liganded oxygen atom, or localized to the dangling oxygen atom. A comparison of the active site carboxylate C-O distances may be able to provide distinction between the three configurations; however, at this resolution, the C-O distances had to be restrained leading to similar C-O distances for all of the active site carboxylates. On the other hand, it may be possible to distinguish between the three double bond configurations by comparing the unrestrained Zn-O distances. Looking at the first coordination sphere oxygens, the carboxylate oxygens of Asp_{117} have short bonds that are similar in length to their corresponding metal ions, indicating that they probably have the same partial charge and that the double bond is most likely shared between them. The inner sphere oxygens from the side chains of Glu_{152} and Asp_{179} also have similar Zn-O distances when compared to each other, but are slightly longer than those of Asp_{117}. This indicates that the distribution of the double bonds for these two side chains is similar to each other, but different than that of the Asp_{117} side chain carboxylate. The double bond most likely is not evenly distributed between the two oxygens, but instead localized to one of the oxygen atoms. One interpretation is that the double bond is localized to the inner sphere oxygens, leaving the dangling oxygens to be either protonated or negatively charged. A second interpretation is that the double bond distribution is localized to the dangling oxygens, and the charge on liganded oxygen is stabilized by its interaction with the metal ion. In the case of AAP, the dangling oxygen of Glu_{152} can potentially form hydrogen bonding interactions with the metal-bridging oxygen of the Tris molecule (3.08 Å), the N_ϵ of His_{256} (3.05 Å), and an active site water molecule (2.72 Å). The dangling oxygen of Asp_{179} can form hydrogen bonding interactions with the alcohol oxygen of Tris that coordinates to Zn_2 (2.95 Å), the side chain oxygen of Ser_{228} (2.58 Å), and the N_ϵ of His_{97} (3.10 Å). In both cases, the potential hydrogen bonding interactions of the dangling oxygens suggest that the double bond is localized to them while the inner sphere oxygens are negatively charged.

A superposition of all atoms in the active sites of the 1.20 Å resolution structure and the 1.8 Å resolution structure overlaid with an rms deviation of 0.12 Å. The structure solved to 1.8 Å resolution in a HEPES buffer showed a network of four water molecules in the active site of AAP, one of which was described as the bridging water species [13](Figure 1). In a Tris buffer, at 1.20 Å resolution, difference Fourier electron density maps with coefficients F_{obs}-F_{calc} and $2F_{obs}$-F_{calc} of the active site clearly showed four connected spheres of electron density in a location similar to that of the water network described in the 1.8 Å resolution structure. A model of Tris, one of the components of the crystallization solution, fits perfectly into the density and was included in further refinement, resulting in a 1% drop in both R_{factor} and R_{free} and improvement in the electron density (Figure 6). Tris was previously reported to be an inhibitor of AAP [21] and the K_i has recently been determined to be 4.65 ± 0.34 mM.

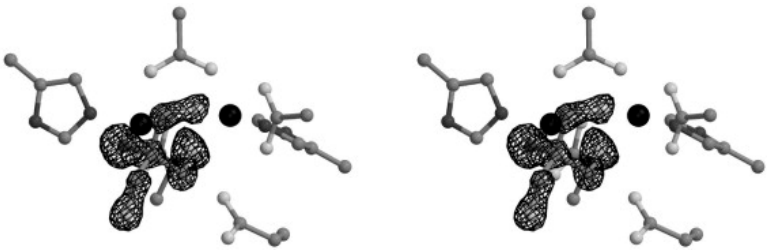

Figure 6. Electron Density for the Active Site Tris Molecule

A schematic of the Tris molecule can be found in Figure 7A.

Tris coordinates to the two metal ions by interactions with three of its functional groups (Figure 7A). An oxygen of Tris bridges the two Zn(II) ions in the position where a bridging water species might be expected. The position of this oxygen is asymmetric with respect to the Zn^{2+} ions. The Zn_1-O distance of 2.21 Å is slightly longer than the Zn_2-O distance of 1.95 Å. A second alcohol oxygen coordinates to Zn_2 with a distance of 2.21 Å. The free amine

of Tris forms another ligand to the catalytic metal ion, Zn_1, with a distance of 2.13 Å. The third oxygen of Tris goes in a direction away from the hydrophobic pocket and shares a hydrogen with the phenolic oxygen of Tyr_{225}.

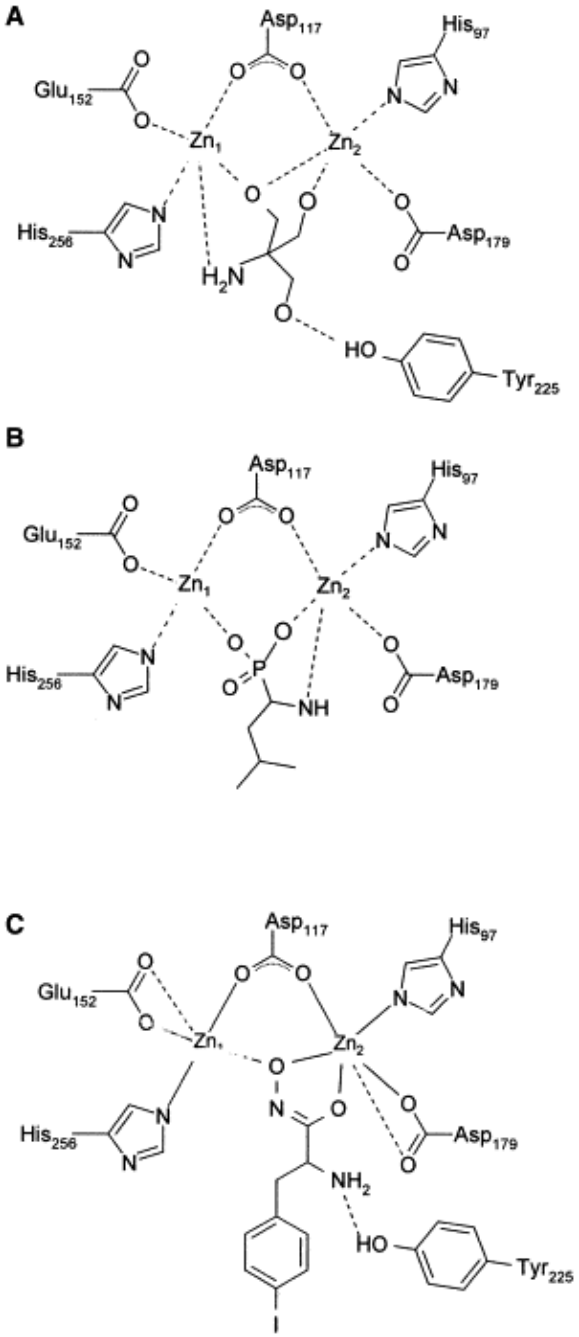

Figure 7. Binding Modes of Tris, LeuP, and IDH

In comparison to the putative transition state analog, leucine phosphonate (Leu-phos) (PDB ID = 1FT7) [17], the binding of Tris is markedly different (Figure 7B). Leu-phos does not contain a metal-bridging oxygen. Instead, a single phosphonate oxygen coordinates to Zn_1, while a second phosphonate oxygen and the free amine coordinate to Zn_2. The Leu side chain is oriented into the hydrophobic pocket, resulting in no interactions with Tyr_{225}. In this orientation, the scissile carbon of the substrate would be in position for attack by the activated nucleophile. The binding mode of Leu-phos in the crystal structure correlates well with the spectroscopic and kinetic analysis of AAP's reaction with substrate in solution.

The binding of Tris to AAP resembles that of *p*-iodo-D-phenylalanine hydroxamate (IDH) (PDB ID = 1IGB) [16](Figure 7C). IDH coordinates with the two metal ions through a bridging interaction of the hydroxamate oxygen, an oxygen ligand from the carbonyl carbon to Zn_2, and an aromatic stacking interaction of the IDH side chain to Tyr_{225}. Tris and IDH have one oxygen that bridges the two metal ions and a second oxygen that coordinates to Zn_2. The side chains of Tris and IDH orient in the same direction in the active site and add stability to their respective enzyme complexes by either hydrogen bonding to the phenolic oxygen of Tyr_{225} in the case of Tris or by an aromatic base stacking interaction in the case of IDH. Thus Tris is not representative of the transition state; instead, it is simply a chelator of the bridged bimetallic center of AAP. This resemblance is not surprising in view of the fact that the binding mode of the hydroxamate inhibitor is primarily directed by the chelating properties of the hydroxamate moiety. The main difference between these two ligands is the interaction of the free amines. This amine coordinates to Zn_1 for Tris and with the phenolic oxygen for IDH.

The difference Fourier electron density map with coefficients $2F_{obs}$-F_{calc} revealed broken electron density around the Tris molecule. The broken electron density can be attributed to an occupancy of approximately 80% for the Tris molecule. A small amount of residual electron density between both metal ions in a position different from the metal-bridging Tris oxygen in the difference Fourier electron density map with coefficients F_{obs}-F_{calc} contoured at 4.5 σ between the two metals was found. The bonding distances from the center of the electron density to the metals are consistent with those previously observed for Zn-O bonds [13]. This electron density accounts for approximately 20% of a residual bridging oxygen species and may be due to a bridging water molecule or hydroxide ion.

Location of Hydrogens

At 1.20 Å resolution it should be possible to locate some hydrogen atoms directly instead of being inferred from bond distances. In the final Fourier difference electron density maps with coefficients F_{obs}-F_{calc}, 999 peaks were identified by Shelx-97 that had not been assigned model atoms. A total of 133 of these were within 0.3 Å of the ideal hydrogen covalent bonding distance of about 1.0 Å for N-H, C-H, and O-H. A total of 108 of the 133 peaks corresponded to carbon hydrogens, with 37% of those belonging to α-carbons. The remaining 25 peaks corresponded to amide nitrogen hydrogen atoms. Two additional peaks were found in positions that are typical for forming hydrogen bonds. All 135 peaks had an electron density level higher than 1.5 σ (0.16 e/$Å^3$) and were found in well-ordered parts of the protein.

Of the two peaks that were found in positions typical of hydrogen bonds, one peak is found 1.14 Å from an imidazole nitrogen of His_{230} and 2.46 Å from the carbonyl oxygen of Tyr_{196}(Figure 8). His_{230} and Tyr_{196} are located in a well-ordered region of the protein. Tyr_{196} is part of a 6 amino acid loop that abuts the α helix containing His_{230}. This hydrogen may form one of the many interactions needed for stabilizing the loop region. The second peak is found 1.74 Å from Asp_{210} and 1.38 Å from Tyr_{218}. Asp_{210} and Tyr_{218} are located in an α helix and a β sheet respectively that are connected by a short 6 amino acid loop.

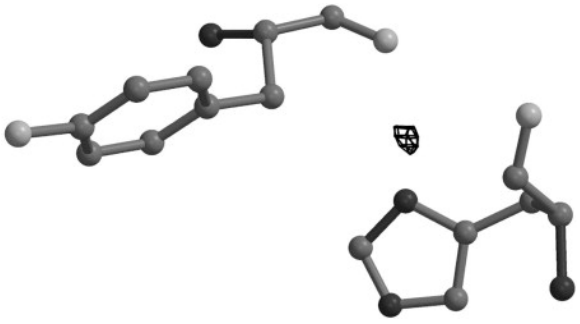

Figure 8. Residual Electron Density in a Fourier Difference Map with Coefficients F_{obs}-F_{calc} Indicative of a Hydrogen Atom

It was hoped that high resolution could reveal the nature of the nonprotein bridge between the two metal ions in the active site. In the native state, the protonation state of the bridging water species is either H_2O or OH^-. The role of Glu_{151} in the mechanism is dictated by the form of this bridging species. In the H_2O form, a hydrogen must be transferred to Glu_{151} in order to activate the water molecule for attack on the substrate carbonyl. If it is in the OH^- form, such a transfer is unnecessary, and Glu_{151} may accept the proton at a later step of the mechanism, after the carbon-nitrogen bond has already been broken, or it may have some other role in the mechanism.

Although the active site is a relatively rigid area of the protein (average B value of 11 $Å^2$ for all of the active site residues compared with 16 $Å^2$ for the rest of the protein), no peaks corresponding to hydrogens were located. This is expected of the Asp, Glu, and His ligands since their side chains are within the first and second coordination spheres of the two metal ions and the pH is above the individual pKas for the liganded amino acid side chains. The bridging water species is present in this structure with only approximately 20% occupancy. Instead, the active site is primarily occupied by a molecule of Tris that forms four contacts with the two metal ions and one contact with an active site residue. The deprotonation of the free amine of Tris requires that the pKa of the hydrogen be lowered from 9.6 to about 6.0. In order to deprotonate the two Tris oxygens that form ligands to the Zn^{2+} ions, the pKa must be lowered from 13.0 to 6.0. For the two Tris oxygens and the free amine that are liganded to the metals, this is certainly possible since single Zn^{2+} ions in proteins are capable of lowering the pKa of a water molecule in bulk solvent from 15.7 to approximately 9.0 [18]. A second metal ion can presumably lower the pKa even further. The third oxygen of Tris may not be deprotonated at all. This oxygen is oriented in the direction of the hydrophobic pocket, and although no electron density has been observed for its hydrogen, the distance of the oxygen atom to the phenolic oxygen of Tyr_{225} is consistent with that observed for hydrogen bonds.

Insight into the Chemical Mechanism

Although none of the active site hydrogens were located in this structure, the binding of Tris adds some insight into the reaction pathway of AAP. In the mechanism proposed by Stamper et al., the roles of Zn_2 were to stabilize the bridging oxygen, to recognize the N terminus of the peptide substrate, to orient substrate, and to stabilize the transition state. If Zn_2 dictated N-terminal recognition and specificity, then one might expect that Zn_2 would coordinate the free amine of Tris. Instead, Zn_1 coordinates the free amine of Tris, indicating that perhaps Zn_2 cannot discriminate between atom types, at least in the absence of the rest of the peptide substrate. One interpretation of these results is that Zn_2 does not play a major role in N-terminal recognition or specificity, but instead, only stabilizes the bridging water molecule. However, the more likely possibility is that Zn_2 plays a role in substrate specificity, but that substrate recognition is primarily directed by the hydrophobic pocket located at the base of the active site [22]. The observation that Tris is a competitive inhibitor of a bridged bimetallic center suggests that the Tris scaffold could be used to design a new family of specific inhibitors for such enzymes.

Biological Implications

The aminopeptidase from *Aeromonas proteolytica* is a bridged bimetallic enzyme that removes the N-terminal amino acid from a peptide chain. Enzymes of this type have been linked to health conditions such as aging, cataracts, inflammation, cystic fibrosis, cancer, HIV infection, and leukemia. Understanding the exact roles of the two metal ions in the chemical reaction pathway of these enzymes is paramount to designing effective drugs that can be used in treatment for such conditions. To fully understand the effects of the two metal ions, one must precisely know where every atom in the active site is positioned, including the active site hydrogens.

The quality of the electron density has led to the discovery of a single Tris molecule chelated to the active site Zn^{2+} ions that is located in a position similar to that of the four water network described in the original structure.

This observation suggests that Tris can be used as a scaffold in the rational design of a new family of specific inhibitors for bimetalloenzymes. Additionally, the quality of the electron density maps allows for the determination of precise atomic positions and can lead to insight into the protonation states of some of the active site amino acid side chains. This information is vital in completely understanding the biochemical reaction mechanism of bimetalloenzymes and in designing specific inhibitors that can interfere with their mode of action.

Experimental Procedures

All chemicals used in this study were purchased commercially and are of the highest quality available. Purified AAP was purchased from Sigma Chemical (St. Louis, MO) as a powder in tricine and $ZnSO_4$. A volume of water was added to the powder, dialyzed 3× against 1 liter volume of 10 mM Tris at pH 8.0, 10 mM KSCN, and 0.4 M NaCl, and concentrated to 16 mg/ml using a Microcon-10 filtration system. The protein was crystallized using the conditions reported previously [23]. 4 µl of AAP (16 mg/ml) in 10 mM Tris at pH 8.0, 10 mM KSCN, and 0.4 M NaCl was crystallized by vapor diffusion using 100 mM Tris at pH 8.0, 100 mM KSCN, and 4.5 M NaCl as the precipitating solution. Crystals with dimensions 0.5 × 0.5 × 0.3 mm^3 were obtained in 48 hr and were shown to be isomorphous with the native crystals obtained from protein that was purified by the previously published method [24].

Diffraction data were collected at the Advanced Photon Source (APS)/BioCARS 14 BM-C station on an ADSC Quantum4 CCD area detector. The X-ray beam had a wavelength of 1 Å, a size of 0.150 × 0.250 mm^2, and was operated at 90–60 mA. An AAP crystal was removed from the hanging drop and flash cooled to −173°C in a stream of nitrogen gas. Data were collected using two sweeps of a single crystal beginning at the same orientation. High-resolution data were obtained using an exposure time of 60 s/frame and a crystal to detector distance of 90 mm. An aluminum attenuator was used to protect the low-resolution region of the area detector. The low-resolution data were collected by reducing the exposure time to 5 s and increasing the sample to detector distance to 150 mm. The sample in each experiment was rotated about its omega axis in 0.5° increments. The data were processed and scaled using DENZO and Scalepack [25]. The data processing and refinement statistics are outlined in Table 2.

Table 2. Crystal Structure and Refinement Statistics

Space group	**$P2_12_12_1$**
Cell dimensions (Å)	a = 67.151, b = 77.025, c = 89.955
Volume fraction of protein (%)	55.24
Vm ($Å^3$/Da)	2.77
Total number residues	468
Total non-H atoms	3654
Number of water molecules	570
Number of zinc atoms	2
Number of inhibitor atoms	15
Temperature factors	
Protein ($Å^2$)	13.566
Solvent ($Å^2$)	27.100
Metal ($Å^2$)	9.185
Inhibitor	12.836
Resolution range of reflections used (Å)	15.0-1.8
R_{factor} (%)[a]	17.43
Free R_{factor} (%)[a]	20.46
Stereochemical ideality	
Bond (Å)	0.009

Angle	1.74°

a

$R_{factor} = \sum|F_o - F_c|/\sum F_o$, where F_o is the observed and F_c is the calculated structure factor amplitude. The R_{free} was calculated for 10% of the reflections excluded from the refinement.

Since this crystal was isomorphous with that of the published native structure (1AMP), the phases from the published native structure were used as the starting model. The two zinc ions and waters were excluded from the original coordinate file. An R_{free} data set was made using 10% of the total unique reflections [26]. The refinement program, CNS [27], was used for a rigid body refinement using reflections from 30.0 to 4.0 Å resolution range and for several rounds of isotropic positional refinement using incrementally higher resolution data to 1.20 Å. The two zinc ions were added after the first positional refinement, and water molecules were added after each round of positional refinement, totaling 50 waters. SHELX-97 [28] was then used for anisotropic refinement, resulting in a 3% drop in the R_{factor} and R_{free}. After each round of refinement, ARP/warp [29] was used to add water molecules. The chemical restraints that are commonly used to refine protein structures were retained throughout the entire refinement procedure. Identification of possible hydrogen positions was performed by utilizing SHELX-97 to generate a Fourier difference map and then searching for electron density peaks within 1.6 Å of any protein atom. The 999 peaks found by SHELXL were then analyzed by comparing the position of the peak with that of the calculated hydrogen position and by measuring the distance between the center of the peak and the associated protein atom. The final R_{factor} of the structure is 14.0% with a R_{free} of 17.6%. A Luzzati plot analysis of atom positions for all atoms is 0.07 Å. The K_i of Tris was determined using a kinetic assay from previously published methods [30].

Acknowledgements

This work was supported by the National Science Foundation (CHE-9816487 to RCH), by the National Institutes of Health (GM26788 to G.A.P. and D.R.), and, in part, by the Macromolecular Training Grant from the NIH (W.D.). Use of the Advanced Photon Source was supported by the U.S. Department of Energy, Basic Energy Sciences, Office of Science, under Contract Number W-31-109-Eng-38. Use of the BioCARS Sector 14 was supported by the National Institutes of Health, National Center for Research Resources, under grant number RR07707.

Accession Numbers

The sequences for E.C. 3.4.11.10 have been deposited in the Protein Data Bank under ID 1LOK.

References

1 N Sträter, W.N Lipscomb, T Klabunde, B Krebs **Two-metal ion catalysis in enzymatic acyl- and phosphoryl-transfer reactions** Angew. Chem., Int. Ed., 35 (1996), pp. 2024-2055

2 D Wilcox **Binuclear metallohydrolases** Chem. Rev., 96 (1996), pp. 2435-2458

3 W.N Lipscomb, N Sträter **Recent advances in zinc enzymology** Chem. Rev., 96 (1996), pp. 2375-2434

4 G Dismukes **Manganese enzymes with binuclear active sites** Chem. Rev., 96 (1996), pp. 2909-2926

5 J Chin **Developing artificial hydrolytic metalloenzymes by a unified mechanistic approach** Acc. Chem. Res., 24 (1991), pp. 145-152

6 K Lai, K Dave, J Wild **Bimetallic binding motifs in organophosphorus hydrolase are important for catalysis and structural organization** J. Biol. Chem., 269 (1994), pp. 16579-16584

7 F Menger, L Gan, E Johnson, D Durst **Phosphate ester hydrolysis catalyzed by metallomicelles** J. Am. Chem. Soc., 109 (1997), pp. 2800-2803

8 V Laurent, D Brooks, D Coates, R Isaac **Functional expression and characterization of the cytoplasmic aminopeptidase p of Caenorhabditis elegans** Eur. J. Biochem., 268 (2001), pp. 5430-5438

9 A Taylor **Aminopeptidases: structure and function** FASEB J., 7 (1993), pp. 290-298

10 A Taylor **Aminopeptidases: towards a mechanism of action** Trends Biochem. Sci., 18 (1993), pp. 167-171
11 G Puldo-Cejudo, B Conway, P Proulx, R Brown, C Izaguirre **Bestatin-mediated inhibition of leucine aminopeptidase may hinder HIV infection** Antiviral Res., 36 (1997), pp. 167-177
12 J Prescott, S Wilkes **Aeromonas aminopeptidase** Methods Enzymol., 45 (1976), pp. 530-543
13 B Chevrier, C Schalk, H D'Orchymont, J.-M Rondeau, D Moras, C Tarnus **Crystal structure of Aeromonas proteolytica aminopeptidase: a prototypical member of the co-catalytic zinc enzyme family** Structure, 2 (1994), pp. 283-291
14 J Prescott, F Wagner, B Holmquist, B Vallee **One hundred fold increased activity of Aeromonas aminopeptidase by sequential substitutions with Ni(II) or Cu(II) followed by zinc** Biochem. Biophys. Res. Commun., 114 (1983), pp. 646-652
15 M Bayliss, J Prescott **Modified activity of Aeromonas aminopeptidase: metal ion substitutions and role of substrates** Biochemistry, 25 (1986), pp. 8113-8117
16 B Chevrier, H D'Orchymont, C Schalk, C Tarnus, D Moras **The structure of the Aeromonas proteolytica aminopeptidase complexed with a hydroxamate inhibitor. involvement in catalysis of Glu151 and two zinc ions of the co-catalytic unit** Eur. J. Biochem., 237 (1996), pp. 393-398
17 C Stamper, B Bennett, T Edwards, R Holz, D Ringe, G Petsko **Inhibition of the aminopeptidase from Aeromonas proteolytica by L-leucinephosphonic acid. Spectroscopic and crystallographic characterization of the transition state of peptide hydrolysis** Biochemistry, 40 (2001), pp. 7035-7046
18 D Christianson, D Cox **Catalysis by metal-activated hydroxide in zinc and manganese metalloenzymes** Annu. Rev. Biochem., 68 (1999), pp. 33-57
19 P Kuhn, M Knapp, S Soltis, G Ganshaw, M Thoene, R Bott **The 0.78 Å structure of a serine protease: Bacillus lentus subtilisin** Biochemistry, 37 (1998), pp. 13446-13452
20 V Kumaraswamy, P Lindley, C Slingsby, I Glover **An eye lens protein-water structure: 1.2 Å resolution structure of B-crystallin at 150 K** Acta Crystallogr. D, 52 (1996), pp. 611-622
21 J Baker, J Prescott **Aeromonas aminopeptidase: pH dependence and a transition-state-analog inhibitor** Biochemistry, 22 (1983), pp. 5322-5331
22 L Ustynyuk, B Bennett, T Edwards, R Holz **Inhibition of the aminopeptidase from Aeromonas proteolytica by aliphatic alcohols. Characterization of the hydrophobic substrate recognition site** Biochemistry., 38 (1999), pp. 11433-11439
23 C Schalk, J Remy, B Chevrier, D Moras, C Tarnus **Rapid purification of the Aeromonas proteolytica aminopeptidase: crystallization and preliminary X-ray data** Arch. Biochem. Biophys., 294 (1992), pp. 91-97
24 G Chen, T Edwards, V D'Souza, R Holz **Mechanistic studies on the aminopeptidase from Aeromonas proteolytica: a two-metal ion mechanism for peptide hydrolysis** Biochemistry, 36 (1997), pp. 4278-4286
25 Z Otwinowski, W Minor **Processing of X-Ray diffraction data collected in oscillation mode** Methods Enzymol., 276 (1997), pp. 307-326
26 A Brunger **The Free R value: a novel statistical quantity for assessing the accuracy of crystal structures** Nature, 355 (1992), pp. 472-474
27 A Brunger, P.D Adams, G.M Clore, P Gros, R.W Grosse-Kunstleve, J.-S Jiang, J Kuszewski, N Nilges, N.S Pannu, R.J Read, *et al.* **Crystallography & NMR system: a new software suite for macromolecular structure determination** Acta Crystallogr. D, 54 (1998), pp. 905-921
28 G Sheldrick, T Schneider The SHELX-97 Manual, IOS Press, Berlin (2001)
29 V Lamzin, K Wilson **Automated refinement for protein crystallography** Methods Enzymol., 277 (1997), pp. 269-305
30 J Baker, S Wilkes, M Bayliss, J Prescott **Hydroxamates and aliphatic boronic acids: marker inhibitors for aminopeptidase** Biochemistry, 22 (1983), pp. 2098-2103